# Evaluation of WRF Parameterizations for Dynamical Downscaling in the Canary Islands

J. C. PÉREZ, J. P. DÍAZ, A. GONZÁLEZ, J. EXPÓSITO, F. RIVERA-LÓPEZ, AND D. TAIMA

*Grupo de Observación de la Tierra y la Atmósfera, Universidad de La Laguna, San Cristóbal de La Laguna, Tenerife, Canary Islands, Spain*

(Manuscript received 2 August 2013, in final form 5 March 2014)

ABSTRACT

The ability of the Weather Research and Forecasting (WRF) Model simulations to perform climate regionalization studies in an orographically complex region, the Canary Islands, is analyzed. Six different 5-yr simulations were carried out to investigate the sensitivity to several parameterization schemes and to uncertainties in sea surface temperature (SST). The simulated maximum and minimum temperatures, together with the daily rainfall, were compared with observational data. To take into account the climatic differences in this archipelago, observational sites were grouped using a geographical regionalization based on principal component analysis and a clustering technique to group the stations according to their climatic characteristics. The analysis showed that both the microphysics and the boundary layer schemes have a large impact on the simulated precipitation. However, the largest differences were observed when the cumulus parameterization, in the coarser domains, was changed. An analysis of the vertical profiles of the simulated hydrometeors was performed to study the differences revealed by the different simulations. Although the cumulus scheme was not applied in the innermost domain, the total amount of water available in the atmospheric column is modified. Moreover, an average increase of 0.7°C in SST, estimated from phase 5 of the Coupled Model Intercomparison Project (CMIP5) variability, produces changes of the same order as those those obtained with different parameterizations. Temperatures are similarly simulated by the different configurations, except for the case in which an SST increment was introduced. Two configurations (CTRL and LSM-PX) were able to correctly reproduce the studied variables in the Canary Islands, improving the Interim ECMWF Re-Analysis (ERA-Interim) data and showing their abilities for regional-scale climate studies in this archipelago.

## 1. Introduction

In recent years global climate models (GCMs) have proven to be a primary effective tool to simulate many aspects of large-scale and global climate, being a key tool for continental and hemispherical climate studies. Although these models incorporate the main characteristics of the general circulation patterns, their applicability to regional climate impact studies is limited because their typical spatial resolutions are on the order of hundreds of kilometers, which is too coarse to provide useful climate information for applications at regional-scale regimes (Leung et al. 2003). Furthermore, at these resolutions, topography is not well represented, which is an additional disadvantage to properly solve the physical processes in some regions, such as in those where mesoscale processes are sensitive to land–sea contrasts or where the orography is complex. To overcome these inconveniences, regional climate models (RCMs) are required, allowing a better and more precise description of those atmospheric events that depend on the orography, land–sea contrast, vegetation cover, and/or land use. Therefore, statistical and dynamical downscaling methods have been developed in recent decades to improve the projections of local climate simulations provided by GCMs (Fowler et al. 2007). Statistical downscaling involves establishing empirical relationships between large-scale climate variables, well represented by GCMs, and local climate variables, often at station level. These methods work by mapping one or more large-scale fields from a reanalysis project to the simultaneous records of finescale observations. They are relatively simple to implement and are computationally cheap. However, statistical downscaling is limited by the assumption of stationarity in the empirical relationships,

*Corresponding author address:* Juan C. Pérez, Grupo de Observación de la Tierra y la Atmósfera, Facultad de Física, Universidad de La Laguna, Avenida Astrofisico Francisco Sánchez s/n, 38206 La Laguna, Santa Cruz de Tenerife, Spain.
E-mail: jcperez@ull.es

DOI: 10.1175/JCLI-D-13-00458.1

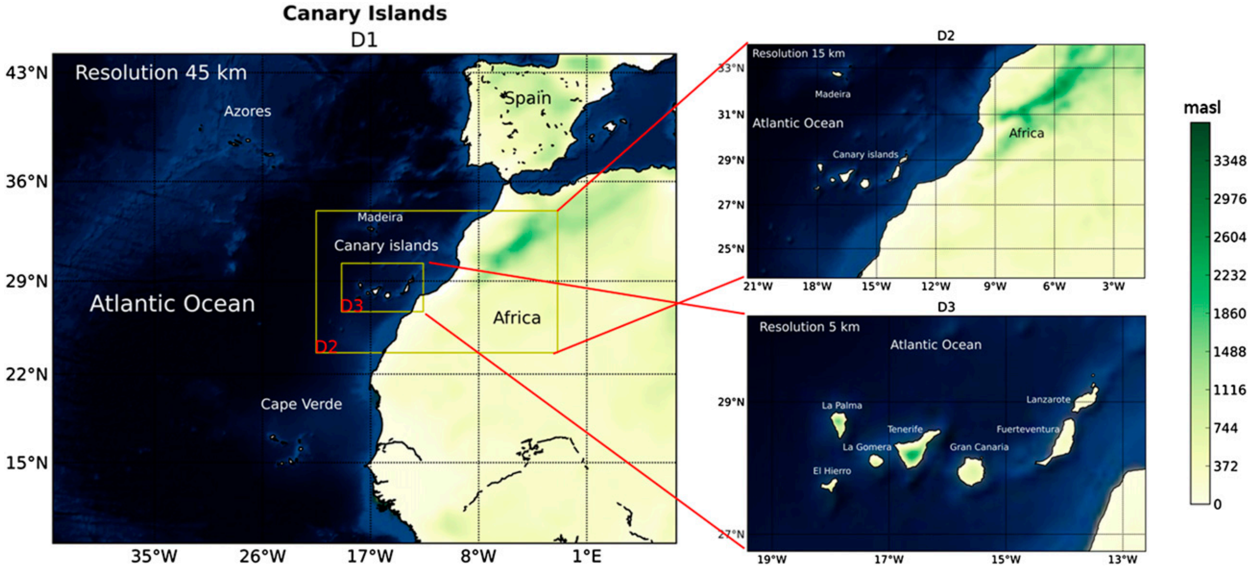


FIG. 1. Domains used in the WRF simulations. The coarse domain (D1) consists of an outer region with 45-km horizontal resolution, a nested domain of 15-km resolution (D2), and an innermost domain (D3) with a resolution of 5 km, covering the Canary Islands.

and results for the present climate do not necessarily translate to forecasts of future climate. On the other hand, the dynamical downscaling techniques are an appropriate alternative to estimating high-resolution regional climatologies. In this approach, RCMs—which are based on the same or similar numerical integration of physical differential equations as those used in GCMs, but over a smaller spatial and temporal domain—are constrained by lateral boundary conditions obtained from GCMs. These methods do not require local observational data and usually outperform statistical methods, particularly regarding the forecast of extreme events (Díez et al. 2005). The major disadvantages of dynamic downscaling methods are their complexity and the required computational power, when compared with the statistical methods, together with the propagation of systematic errors transferred from GCMs to RCMs (Giorgi et al. 2001). One of the latest generation of mesoscale models is the Weather Research and Forecasting (WRF) Model (Skamarock et al. 2008), which became popular since it is a freely available open source model and offers a large amount of physical possibilities. It is a nonhydrostatic model, based on the fifth-generation Pennsylvania State University–National Center for Atmospheric Research (NCAR) Mesoscale Model (MM5; Grell et al. 1995); it is suitable for simulating a wide range of scales, from thousands of kilometers to a few meters; and it is also commonly used for modeling climate, and for chemistry and air quality research and prediction. The large number of available options for physical parameterizations (radiation, cumulus schemes, planetary boundary layers, microphysics, and surface models), makes it flexible and appropriate for climate research. WRF has been successfully used to perform studies ranging in time scale from specific cases (Chang et al. 2009; Evans et al. 2012) to decades (Evans and McCabe 2010; Nikulin et al. 2012; Yuan et al. 2012), including seasonal (Crétat et al. 2012; Flaounas et al. 2011) and annual studies (Lo et al. 2008; Pohl et al. 2011; Suklitsch et al. 2011).

A first objective of RCMs is to find a consistency between simulated physical parameters, such as temperature and precipitation, and observational data. Thus, the research community has focused its efforts on bridging the gap between the RCM simulations and the actual climate of a region. One of the main difficulties of local climate studies using RCMs is the characterization of complex areas. From a climatological point of view, the Canary Islands can be considered as a complex region, given their location (Fig. 1) and their orography, with altitude variations of more than 3000 m in less than 20 km horizontally, which makes the archipelago an interesting area to investigate a wide variety of meteorological and climate issues (González et al. 2013). This complexity has been shown in previous studies, such as the climate atlas of the Canary Islands elaborated by AEMET and IPMA (2012). In that work, specifically in their Fig. 5, the inhomogeneous geographical distribution of the annual mean temperature can be observed, showing a clear dependence on the elevation and on the orientation of the slopes, with the northern-oriented, windward areas being colder than the southern parts, mainly in those islands with high relief. The distribution of the observed precipitation is also very dependent on the orography (AEMET and IPMA 2012, see their Fig.

60). Canary Islands climate, influenced by the trade wind belt, is usually very stable and dry, and rainy events only occur when disturbances break the quasi-permanent thermal inversion layer, with topography being the main factor that affects the local rainfall distribution (García-Herrera et al. 2001). In the northern ridges of the high-relief islands annual precipitation amounts around 1000 mm are observed, while in the southern parts of these islands or in the flatter, eastern islands the mean annual precipitation is around 200 mm. These orographic effects are observed at spatial scales much smaller than those resolved by global atmospheric models. Therefore, the use of mesoscale models, with a more realistic representation of the complex terrain and heterogeneous land surfaces, is needed (Dulière et al. 2011).

In this study, WRF has been used to perform 5-yr simulations, from 2004 to 2008, with a horizontal resolution of 5 km, downscaling Interim European Centre for Medium-Range Weather Forecasts (ECMWF) Re-Analysis (ERA-Interim) data (Dee et al. 2011) to the Canary Islands region, centered at 28°N, 16°W. The main aim of this work is to examine the ability of WRF simulations to reproduce the available observations of precipitation and temperature obtained from weather stations in order to select an adequate configuration that allows us, in a first step, to quantify model uncertainties when accurate initial and boundary conditions are provided by reanalysis data and, after that, to perform projection runs for this area. The paper is structured as follows. In section 2, the model setup is described for the different WRF physical configurations. The observational data and their geographical regionalization are described in section 3. In section 4, the results of the different simulations over each region are discussed and compared with the observational and reanalysis datasets. A final section summarizes and provides conclusions about the main findings of this work.

## 2. Model setup

As previously mentioned, the WRF version 3.4.1 was used to perform the simulations of dynamical downscaling, using three domains in a double nested configuration. As can be seen in Fig. 1, the coarse domain (D1) covers the Canary Islands, the Iberian Peninsula, and part of the West African continent, covering the latitude and longitude coordinates 8.41°–44.13°N, 43.46°W–8.46°E. This outer domain has been configured using 100 × 88 grid cells with 45 km of horizontal resolution. The first nested domain (D2), with a resolution of 15 km and 127 × 73 grid cells, covers the geographical range 23.64°–33.00°N, 21.53°E–1.43°W. The innermost domain (D3) covers the seven islands of the archipelago, and is located within 26.74°–30.28°N, 19.42°–12.61°W. This domain has a horizontal resolution of 5 km and 133 × 79 grid cells. A 3:1 grid ratio for the nested domains has been selected because it has been extensively tested and is considered the optimal relation for the mesh refinement. The employed nesting method was one-way, in which outputs of the outer domain are interpolated to the nest domain as boundary conditions for driving, once the coarser domain simulation has finished (Soriano et al. 2002). The term ''one way'' alludes to the fact that there is not feedback from the inner domain to the coarse domain, avoiding possible pollution when resolving equations of the models in parent domain. The time steps selected for the different domains were 225, 75, and 25 s, respectively, and all of them have been discretized with 32 vertical eta levels. Simulation outputs were sampled every 2 h for the whole simulation time. This work focuses on high-resolution simulations, so only the 5-km domain is analyzed.

The initial and boundary conditions for WRF simulations were obtained from data of the ERA-Interim, the latest and most advanced global atmospheric reanalysis produced by the ECMWF. ERA-Interim is an improved version of the previous generation 40-yr ECMWF Re-Analysis (ERA-40) data, presenting a longer time range, a better assimilation scheme, an updated physical package, more vertical levels, and higher resolution (Simmons et al. 2006). The ERA-Interim data employed in present work were gridded to 0.75° × 0.75° spatial resolution, with 32 vertical pressure levels, and are available with a frequency of 6 h. Recent studies have shown that ERA-Interim provides a better representation of certain variables than other reanalysis data (Mooney et al. 2011).

In the process of dynamical downscaling, ERA-Interim provides the initial and boundary conditions to the RCM. As the simulation evolves, the internal solution computed by the RCM diverges from the driving analysis. To avoid these errors, a grid analysis nudging technique was applied (Stauffer and Seaman 1990), controlling the deviation of the RCM from the GCM in the spatial scales typical of the GCM (Radu et al. 2008) and eliminating the effects of domain position and geometry in regional climate model simulations (Miguez-Macho et al. 2004). The nudging technique adds an additional term to the equations of motion that reflects the difference between the observed state and the model state at a given location and time. Only the outer domain (D1) is nudged in order to let the regional model create its own structures in the higher-resolution inner domains. For the same reason, nudging is applied only on vertical levels above the boundary layer.

TABLE 1. Summary of WRF parameterization schemes used in this study.

| Scenario | MP | PBL | LSM | CP | Radiation | SST |
|---|---|---|---|---|---|---|
| CTRL | WDM6 | YSU | Noah | KF | CAM3 | ERA-Interim |
| MP-THOM | THOM | YSU | Noah | KF | CAM3 | ERA-Interim |
| PBL-MYJ | WDM6 | MYJ | Noah | KF | CAM3 | ERA-Interim |
| CU-TI | WDM6 | YSU | Noah | TI | CAM3 | ERA-Interim |
| LSM-PX | WDM6 | YSU | PX | KF | CAM3 | ERA-Interim |
| DSST | WDM6 | YSU | Noah | KF | CAM3 | ERA-Interim + ΔCMIP5 |

All the WRF simulations were initialized on 1 January 2003 and integrated until 31 December 2008. The first year is considered as the model spinup to ensure model equilibrium between external forcing and internal dynamics (Hamdi et al. 2014). Taking into account that the spinup may disturb the model results, this period is excluded from further analysis.

For this study, five WRF simulations, using different parameterizations, have been performed to study their effects on temperature and precipitation in the Canary Islands. These different scheme combinations were selected considering previous results for the same area using a larger set of WRF simulations for shorter periods and other variables, such as precipitable water vapor (González et al. 2013). These combinations are summarized in Table 1. As can be seen in this table, for all experiments, radiation schemes were set to the Community Atmosphere Model, version 3 (CAM3), for computing both longwave and shortwave radiation fluxes (Collins et al. 2004). Radiation schemes control the energy balance between heating from sunlight and cooling by infrared. They also take into account the role of clouds reflecting and scattering energy in both directions.

For the cumulus parameterization (CP) in the outer domains, D1 and D2, the Kain–Fritsch (KF) (Kain and Fritsch 1990) and the modified Tiedtke (TI) (Zhang et al. 2011) schemes were chosen. CP specifies how to handle cumulus clouds that are too small to be directly resolved by the model, intending to represent vertical fluxes due to unresolved updrafts and downdrafts and compensating motion outside the clouds. No cumulus parameterization was applied in the innermost region (D3) because the fluxes can be explicitly resolved at resolutions under 10 km (Skamarock et al. 2008).

The planetary boundary layer (PBL) was characterized using the Yonsei University (YSU) (Hong et al. 2006) and Mellor–Yamada–Janjić (MYJ; Janjić 2002) schemes. PBL schemes are used with the aim of parameterizing the turbulent vertical fluxes of heat, momentum, and constituents such as moisture within the PBL and throughout the atmosphere. The MYJ scheme is a local closure model where the vertical turbulent diffusivity is calculated based on the local turbulent kinetic energy (TKE) equation. In this scheme, entrainment is implicitly treated. The YSU scheme is a nonlocal model and considers the fluxes implicitly, through a parameterized nonlocal term. In this case, entrainment is explicitly treated.

For the land surface processes, the Noah (Chen and Dudhia 2001) land surface model (LSM) is used in all simulations except one, where the Pleim–Xiu (PX) LSM (Xiu and Pleim 2001) is used. The LSM provides the features of the land surface and therefore plays an important role in simulating soil temperature, moisture profiles, and canopy properties. For this reason, a good characterization and parameterization of land surface processes through LSMs enhances the numerical regional climate simulations, reducing the uncertainties. The Noah LSM is based on the concept that a LSM should be able to provide not only reasonable diurnal variations of surface sensible and latent heat fluxes as surface boundary conditions for coupled models, but also correct seasonal evolutions of soil moisture in the context of a long-term data assimilation system. It includes root zone, evapotranspiration, soil drainage, and runoff, taking also into account vegetation categories, monthly vegetation fraction, and soil texture. The PX LSM includes explicit soil moisture and evapotranspiration based on the interactions between the soil, biosphere, and atmosphere and the nonlocal PBL model. The three pathways of evaporation computed are the direct soil evaporation, the canopy evaporation, and the vegetative evapotranspiration.

The WRF double-moment six-class (WDM6) (Lim and Hong 2010) and Thompson (THOM) (Thompson et al. 2008) models were used as cloud microphysics (MP) schemes. The cloud microphysics model controls how water in its various phases (rain, vapor, ice, cloud droplets, etc.) are treated. Clearly, the choice of a specific microphysical scheme affects directly the details of cloud physics. The scheme WDM6 is the extended version of the WRF single-moment six-class (WSM6) (Hong and Lim 2006) and, in addition to the prediction for the mixing ratios of six water substances (water vapor, cloud droplets, cloud ice, snow, rain, and graupel), it includes the prediction of the number concentrations for cloud and rainwater, providing an additional prognostic variable, the number concentration of the cloud condensation nuclei (CCN). The THOM scheme is also a double-moment scheme, which predicts the mixing ratio for five hydrometeors and the number concentration of ice phase hydrometeors and rain.

The use of reanalysis fields for evaluating the mesoscale models allows us to isolate the skills of the regional models, assuming that errors in the large-scale climatology from the reanalysis are small (Dulière et al. 2011). However, for climate projections studies, any uncertainty in the fields used as boundary conditions will affect the simulated variables. In contrast to continental areas, uncertainties in sea surface temperature (SST) could have a considerable impact in the studied region because a large portion of the domains used in the simulations corresponds to ocean surface. Furthermore, the WRF parameterizations treat ocean areas very crudely, so the sea surface conditions must be provided by large-scale models or by analysis data, as is the case of this work where ERA-Interim is used. Although the main aim of this work is to evaluate the skills of WRF simulations, a sixth experiment (DSST) was performed to study the effects of SST uncertainties on temperature and precipitation. To this end, 13 models belonging to phase 5 of the Coupled Model Intercomparison Project (CMIP5) were selected and their historical runs, from 1980 to 2005, were evaluated to compute the monthly standard deviation of the SST provided by this set of models. Then, this uncertainty signal, with an average value of 0.7°C and representative of the variability of the different global climate models, was added to the ERA-Interim data to provide the new SST conditions used by the mesoscale model during the simulation period.

## 3. Observational data and geographical regionalization

Temperature and rainfall simulated outputs were validated with observational records obtained from the Spanish Meteorological Agency [Agencia Estatal de Meteorología (AEMET)]. These data consist of hourly temperature and daily precipitation series from 50 and 51 surface stations, respectively. From all these stations, those with more than 10% of missing values for the selected period were discarded for the comparative study. So, taking into account these criteria, 23 and 22 useful precipitation and temperature stations were finally available, respectively.

The archipelago under study is located in the Atlantic Ocean, just off the northwest African coast, at about 100 km west of the border between Morocco and the Western Sahara. It consists of seven volcanic islands: Tenerife, Fuerteventura, Gran Canaria, Lanzarote, La Palma, La Gomera, and El Hierro (Fig. 1). The landscape of each island is very different from the others, so there is a great diversity of ecosystem regions, from the humid forests on Tenerife and La Palma to the sand dunes in Gran Canaria and Fuerteventura. The consequences are special environmental conditions, where the orography modifies the climatic conditions at a local level, producing a significant variety of microclimates, and giving place to numerous different climactic zones within relatively small distances. The effects of the cold Canaries ocean current, the persistence of trade winds, and the abrupt orography cause the western islands to be wetter than other territories located at similar latitude.

The results of the different WRF experiments can be better understood if observational sites are grouped in climatic homogeneous subregions using regionalization techniques. Originally, some empirical methods based on thresholds applied to several variables, such as temperature, precipitation, and/or evapotranspiration, were used to estimate the climatic regions (e.g., Köppen 1936; Thornthwaite 1948). For example, AEMET and IPMA (2012) used a Köppen–Geiger climate classification in the atlas for the archipelagos of the Azores, Madeira, and the Canary Islands. However, during the last decades, objective regionalization methods, for different climatic variables, have been developed and applied to many regions of the world. These methods are mainly based on principal component analysis (PCA) and/or clustering analysis (CA) (Jiménez et al. 2008).

In this work, a two-step methodology, with a consecutive application of PCA and CA algorithms, similar to that proposed by Argüeso et al. (2011), has been applied to determine the climatic regions for temperature and precipitation in the Canary Islands. In both cases, as the first step, the S-mode PCA was computed using the covariance matrix obtained from daily values over the period 2004–08 to reduce the original dataset by eliminating part of their redundancy. Some of the most common rules to determine the optimal number of significant principal components (Wilks 2005) were checked for precipitation and temperature. However, because of the number of available meteorological stations and the previous knowledge about the climatology on the fragmented territory that forms the archipelago of the Canary Islands, the final number of significant components was manually selected from those suggested by these methods, resulting in a coherent classification of the different sites after the CA application, as explained below.

Once the principal components have been computed, a CA is applied for grouping those sites that have some

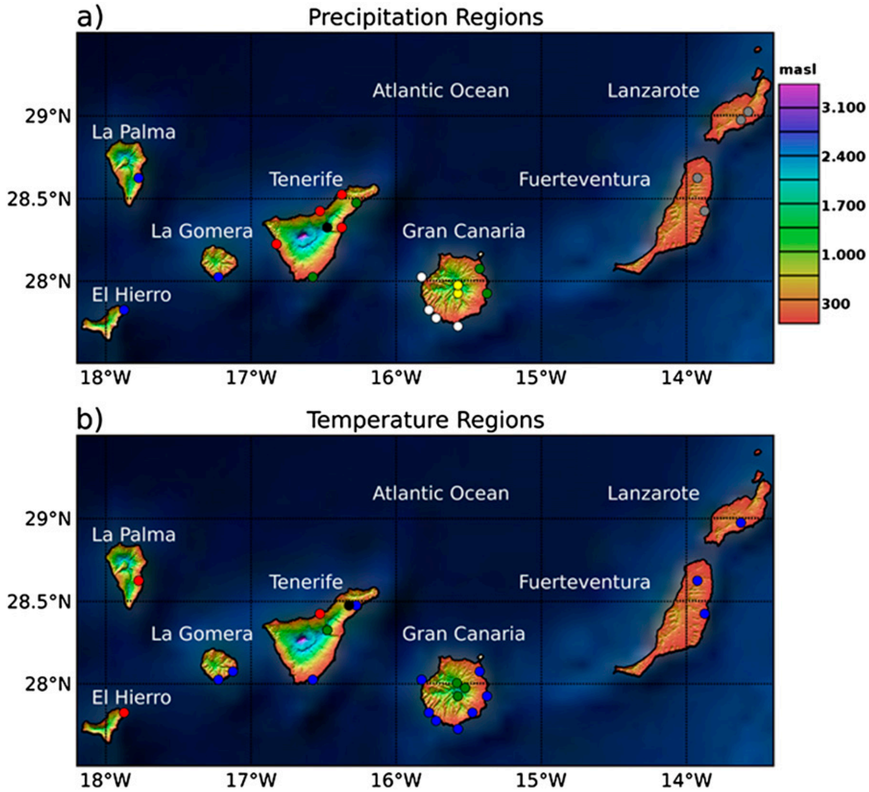


FIG. 2. (a) Precipitation and (b) temperature regionalization maps. Colored points represent the geographical position of the observational stations. Precipitation regions are identified as follows: Region 1 (blue), La Palma, La Gomera, and El Hierro airports; region 2 (red), north Tenerife; region 3 (green), southeast Tenerife and east Gran Canaria; region 4 (black), Izaña observatory; region 5 (yellow), high-altitude Gran Canaria; region 6 (white), southwest Gran Canaria; and region 7 (gray), Lanzarote and Fuerteventura islands. Temperature regions are identified as region 1 (blue), low altitude; region 2 (red), La Palma, north Tenerife, and El Hierro; region 3 (green), Izaña observatory and high-altitude Gran Canaria; and region 4 (black), Los Rodeos airport.

natural relation between them. There are two basic types of CAs, partitioning and hierarchical algorithms, both with their own advantages and shortcomings (Kaufman and Rousseeuw 1990). In this work, a method based on the density-based spatial clustering of applications with noise (DBSCAN) algorithm has been selected on account of its properties (Ester et al. 1996): it discovers clusters of arbitrary shapes, not only convex clusters as is the case for the majority of CAs; it requires only one input parameter, which fixes the radius around a point in the features space that must contain at least another member of the same cluster; and it does not require an a priori knowledge about the number of clusters contained in the dataset. Specifically, a version proposed by Daszykowski et al. (2001) has been used, because they implemented an algorithm to estimate the required parameter based on statistical considerations.

When the proposed methodology was applied to precipitation data, using five principal components, six different clusters were obtained. Additionally, a site was classified as an outlier and was considered as an additional region (Fig. 2a, black circle). This site corresponds to the GAW (Global Atmospheric Watch) Izaña observatory (www.izana.org), located at 2367 m above mean sea level (MSL) on the mountain ridge that crosses the island of Tenerife from the center to the northeast. The other six groups are the three stations located at the airports of the western islands, that is, La Palma, La Gomera, and El Hierro; those sites in Tenerife, the highest island, which are more affected by orographic precipitation (red circles); the four sites located on the southeastern coasts of Tenerife and Gran Canaria (green circles); the four stations on the southwestern coast of Gran Canaria (white circles); the three stations located at high altitude, above 1800 m MSL, in the central part of Gran Canaria (yellow circles); and the four sites on the two eastern islands (gray circles).

The case of temperature is simpler than the precipitation regionalization. Thus, only three principal components were necessary and four regions were obtained. The same clusters were obtained for minimum and maximum temperature datasets; they are (Fig. 2b) the three low-altitude stations located in El Hierro, La Palma, and the northern coast of Tenerife (red circles); the rest of the sites located at low altitude (blue circles); the four high-altitude sites in Gran Canaria and Tenerife (green circles); and the Los Rodeos airport station (black circle), which was classified as an outlier and which is located at 630 m MSL in a valley that connects the north and the south slopes of the island, being directly affected by stratocumulus clouds (Martín et al. 2012), mainly during the summer where the trade winds are more persistent (Font-Tullot 1956).

## 4. Model evaluation

The following subsections present the obtained WRF outputs for the different experiments, compared with the available observational data, in order to evaluate the skills of the simulations. ERA-Interim data are also considered. Results are presented using the regions that were obtained through the previously mentioned method, for precipitation (seven regions) and temperature (four regions). Minimum and maximum temperatures and rainfall percentiles were calculated for each region. In addition to percentiles, the annual cycles from monthly averages are presented for these variables in order to evaluate WRF simulation skills in reproducing seasonal behavior. Finally, Taylor diagrams (Taylor 2001) are displayed to summarize other statistical parameters, such as the correlation coefficient, the standard deviation, the root-mean-square error (RMSE), and the bias, to determine, together with the percentiles and annual cycles, the WRF configuration that best fits the observed temperature and precipitation in the Canary Islands.

### *a. Daily precipitation results*

To analyze the intensity of daily precipitation, the 50th, 60th, 70th, 75th, 80th, 90th, 95th, and 99th percentiles were computed, taking into account rainy days defined by a 0.1 mm day$^{-1}$ threshold, according with the resolution of the observational stations. The results are shown in Fig. 3, where the WRF percentiles are plotted versus the observational data for each region, taking the simulation grid point nearest to each station. The blue line represents a perfect performance, indicating the over- or underestimation of the simulations. Percentiles obtained from ERA-Interim are also displayed, and, as can be expected, WRF simulations outperform ERA-Interim because of the lower resolution of ERA-Interim, leading to a misrepresented orography that reduces its effect on precipitation, underestimating the rainfall events in all regions. Analyzing the seven regions under study, the control (CTRL), CU-TI, and LSM-PX simulations follow the observational percentiles quite well if compared with the MP-THOM and PBL-MYJ. The experiments MP-THOM and PBL-MYJ underestimate rainfall in all the areas. CU-TI reproduces remarkably well all the percentiles under 80% (except for region 4, Izaña), overestimating extreme precipitation episodes (99%) in regions 2, 4, 6, and 7. The CTRL and LSM-PX schemes tend to slightly underestimate precipitation under 80% (except for region 4) and in some regions the simulations of the 99% extreme coincide exactly with the perfect performance (e.g., the LSM-PX experiment in regions 6 and 7). The results indicate that although the WRF dynamical downscaling has the capability of reproducing rainfall better than ERA-Interim, extreme rainfall events are still difficult to reproduce, as indicated by the high percentile values. In conclusion, microphysics and PBL parameterizations affect strongly the rainfall simulations. The LSM-PX scheme does not present great discrepancies if compared with CTRL simulation because the only difference between both simulations is the selected LSM (Noah in CTRL and PX in LSM-PX). The results indicate that precipitation is less sensitive to the chosen LSM, probably because only a small percentage of the simulation domain (D3) is covered by land. This figure also shows that the increase in the prescribed SST causes an increment in the simulated precipitation. However, this increment is not homogeneously distributed for the different regions, obtaining the largest differences for the highest altitude site, region 4, and for the extreme episodes.

To understand the large differences in the simulated precipitation between the experiments, a more detailed study was performed to analyze the behavior of the different runs. Figure 4 shows the mixing ratio vertical profiles of the condensates provided by the different simulations, corresponding to the winter season, when the rainfall events are predominant in this archipelago. These profiles were generated by averaging the vertical distribution over all land grid points that cover Tenerife, which is the island with the most complex orography and the largest climatic contrasts in the archipelago. From this figure, it can be observed how the vertical distribution of cloud water is similar in the different runs except when the Thompson microphysical scheme is used. In this case, although the main cloud deck located at

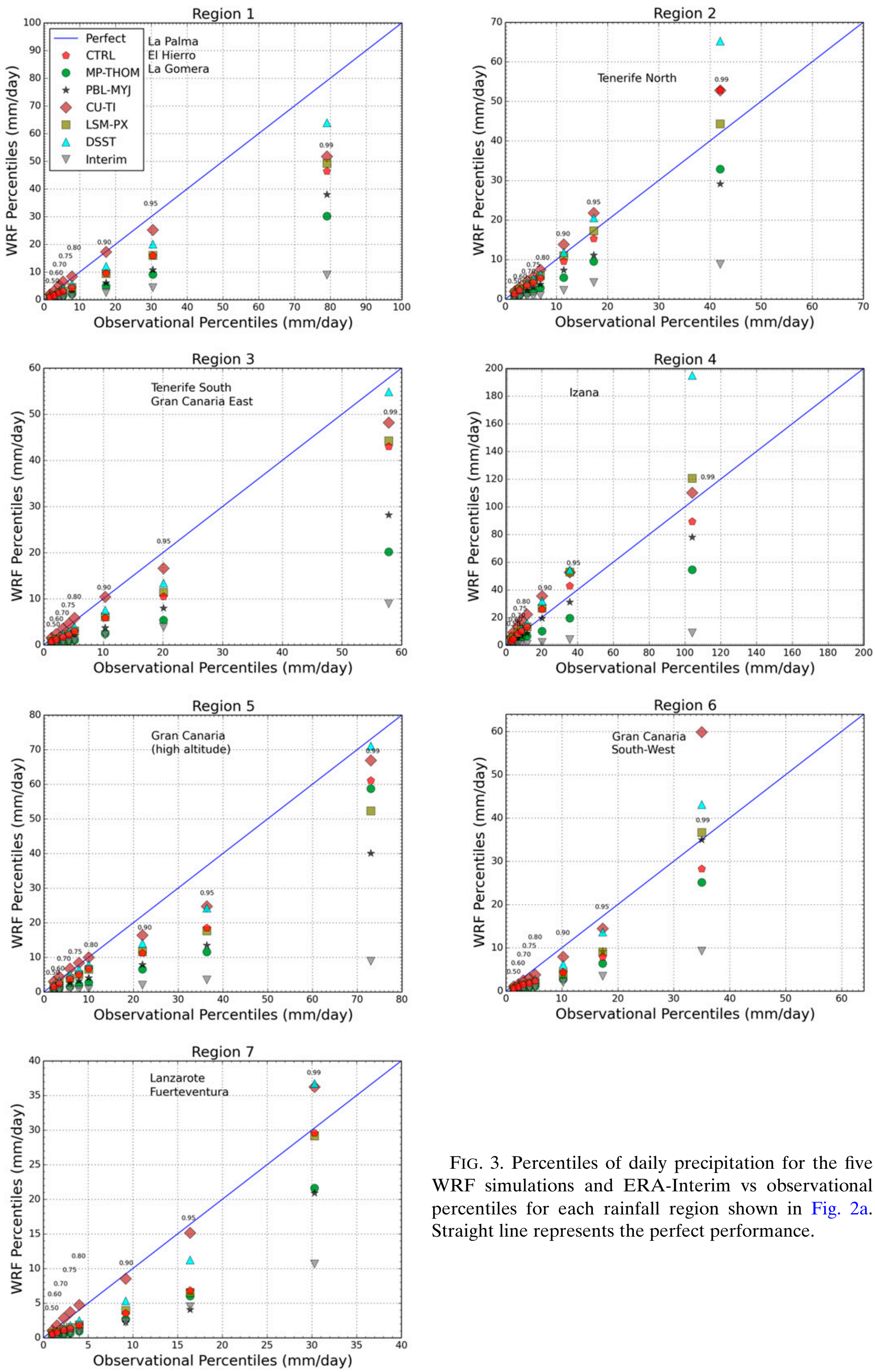


FIG. 3. Percentiles of daily precipitation for the five WRF simulations and ERA-Interim vs observational percentiles for each rainfall region shown in Fig. 2a. Straight line represents the perfect performance.

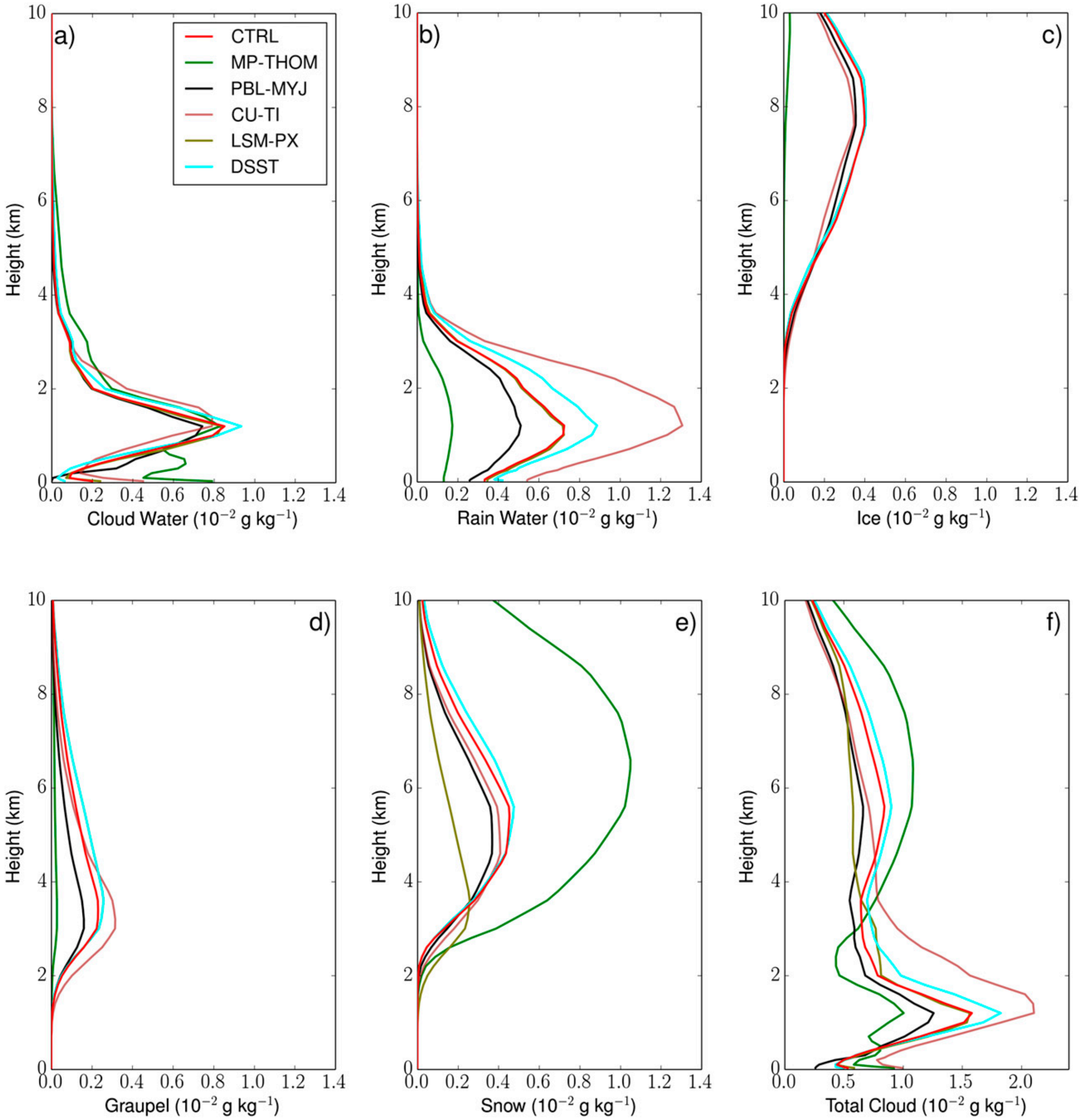


FIG. 4. Spatial and temporal means of mixing ratios vertical profiles of the condensates provided by the different schemes, corresponding to the winter season and computed for Tenerife island: (a) cloud water, (b) rainwater, (c) ice, (d) graupel, (e) snow, and (f) total condensate.

around 1500 m MSL is also reproduced, a new layer appears at very low levels, which is also revealed when the vertical profile of cloud fraction is analyzed (not shown). However, this distribution contrasts with the results obtained for the rainwater specie, where it can be appreciated how the amount of this condensate varies drastically from the lower values provided by the Thompson scheme (MP-THOM) to the simulations carried out using the Tiedtke cumulus parameterization (CU-TI) in the outer domains, which provide values one order of magnitude larger for this condensate. Also remarkable are the differences obtained for the ice, snow, and graupel species for which the Thompson scheme seems to be very efficient in producing snow in the midtroposphere at the expense of ice and graupel (Figs. 4c–e).

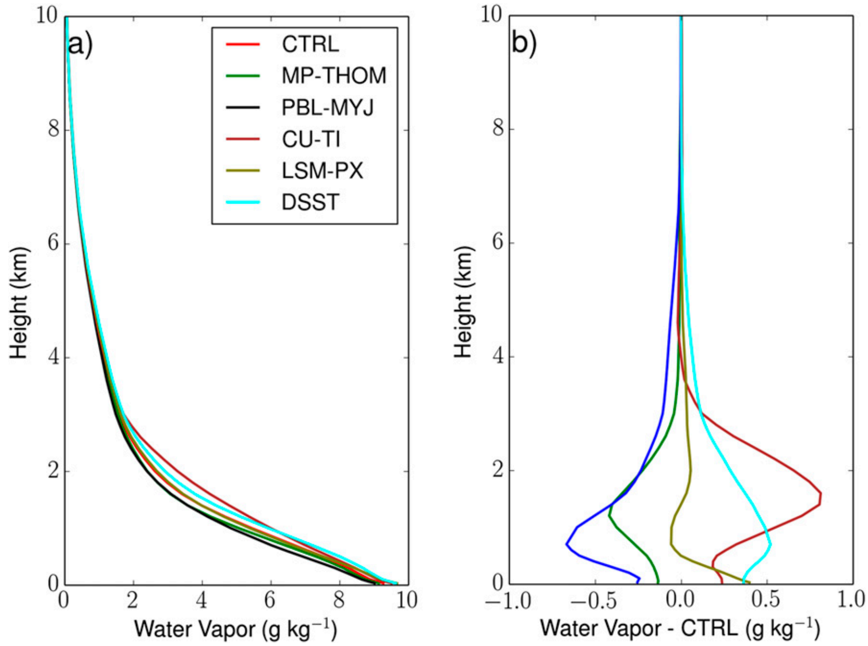


FIG. 5. (a) Spatial and temporal mean profiles of winter water vapor mixing ratio for the five experiments and Tenerife island and (b) the differences with CTRL experiment.

Moreover, if the differences in water vapor mixing ratios of the other simulations with the control experiment are analyzed (Fig. 5b), it can be noticed how the amount of water available in the experiment CU-TI, both as water vapor (Fig. 5) or as the sum of the different cloud condensates (Fig. 4f), is larger than in the other simulations. This shows that, in spite of the fact that cumulus parameterizations are not applied in the innermost domain, when the Tiedtke scheme is used in the outer domains, it provides larger amounts of water to the high-resolution domain. When the microphysics processes are considered the excess of water is redistributed between the different species, leading to larger amounts of precipitation. In a similar way, in the simulation with larger values of SST, the total amount of water vapor in the lower layers also increases, which in turn produces larger amounts of precipitation.

Furthermore, these figures also show that when the YSU PBL scheme is used, the total amount of water vapor available in the lower levels, as well as the total cloud mixing ratio, is larger compared to the MYJ scheme, which can be due to the upward moisture surface flux, which in these simulations is 15% higher when YSU parameterizations are used.

Concerning the experiment LSM-PX, as could be expected in a territory with small land area, the behavior is similar to the control simulation. The only appreciable difference appears in the total water vapor amount near the surface due to different treatment of the moisture fluxes, but no remarkable differences are found in the distribution of cloud species.

### *b. Annual cycle for precipitation*

The annual cycles of the simulated precipitation are presented in Fig. 6, together with the observational and the ERA-Interim data. The seasonal pattern is, in general, well captured by the simulations, showing highest precipitation during winter and lowest during summer, with clear discrepancies in the rates (under- or overestimation depending on the considered simulation) with respect to the observational data.

All the experiments capture the dry months, between June and August, accurately. The CU-TI scheme clearly overestimates rainfall in all regions (Fig. 6), as previously discussed. In the percentiles figure (Fig. 3), this behavior is not clearly appreciated, and it can be explained by the fact that in the study annual cycles included 100% of the simulation data, whereas the case of percentiles does not include the data between the 99th and 100th percentiles. After revision of the results it has been checked that the overestimation is mainly due to very intense precipitation episodes that fall over the 99th percentile. For the other simulations, and with regard to seasonal behavior, it is very difficult to discern which one simulates better the observational rainfalls. The modeling of precipitation is one of the main challenges in high-resolution regional models. Indeed,

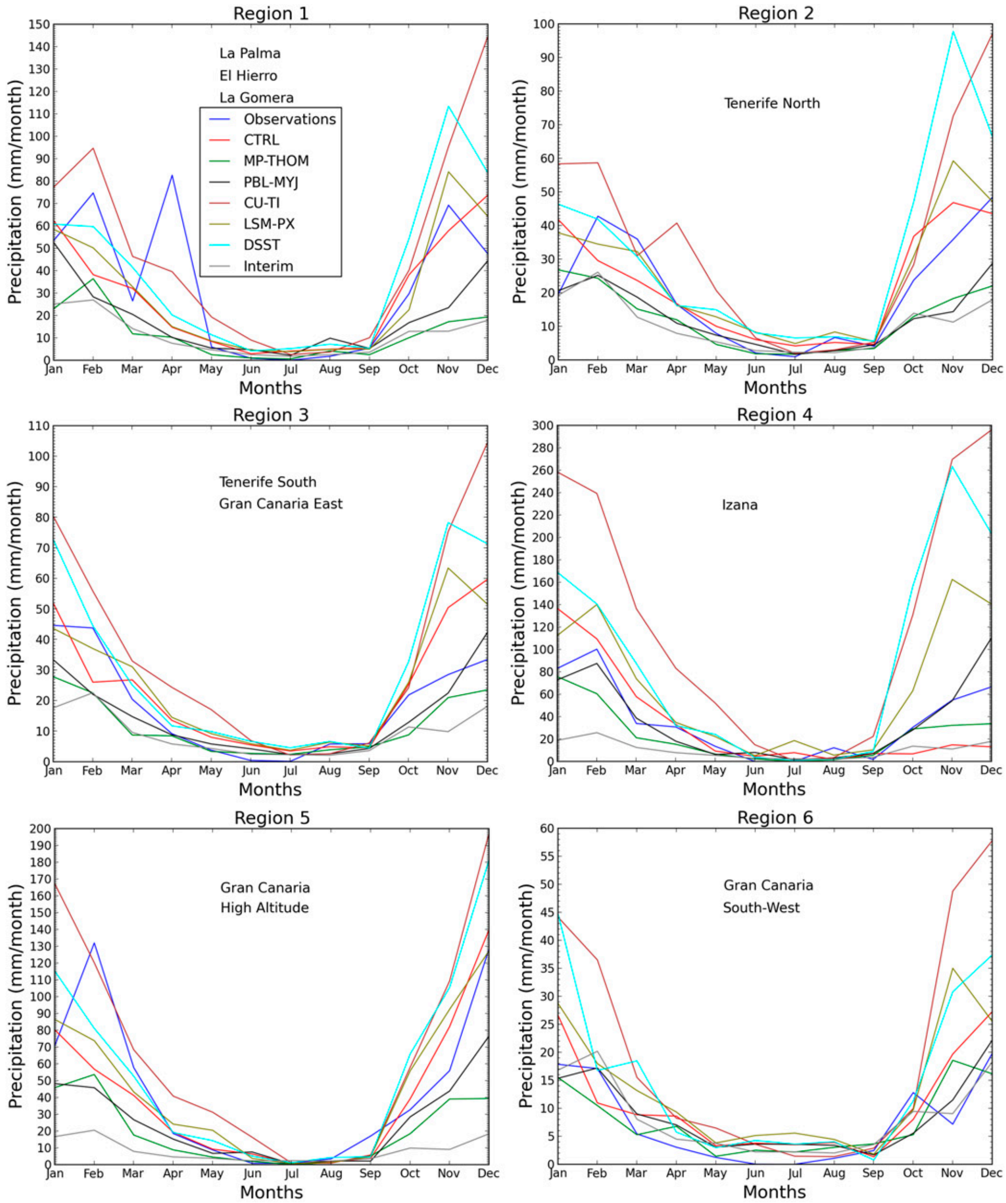


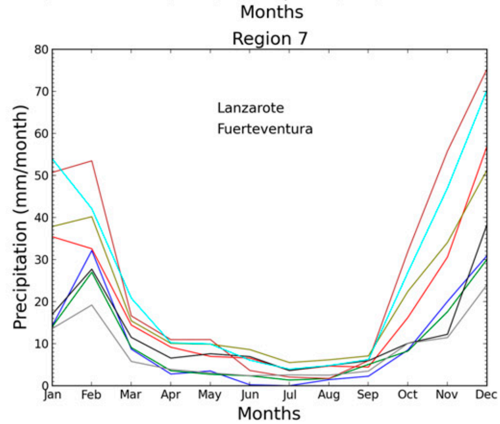


FIG. 6. Annual cycle of monthly precipitation for the different regions shown in Fig. 2a.

simulations results of precipitation are less reliable compared with temperature. This is because rainfall is more heavily affected by nonlinear processes, which are not yet well characterized in present regional climate models. However, all the simulations outperform precipitation outputs from ERA-Interim, which tends to underestimate the rainfall in all regions except region 6. Large differences in the amount of precipitation between plain areas and higher elevations is observed, with maximum values around 80–120 mm month$^{-1}$ in Izaña (Tenerife) and Gran Canaria mountainous areas, corresponding to regions 4 and 5, respectively. Higher elevation leads to increased vertical lift and precipitation rates due to orographic enhancement. This is evident because in the Canary Islands the precipitation events are dominated by the orographic effects (Font-Tullot 1956; García-Herrera et al. 2001). A clear example of this situation can be observed in region 7, which comprises Lanzarote and Fuerteventura islands, where the low orography causes the low rainfall episodes observed, more similar to other areas at the same latitudes.

Figure 7 shows the geographical distribution of simulated mean annual precipitation and the importance of grid resolution, using CTRL experiment results. It can be appreciated how the relatively small size of the islands and their complex orography make it necessary to use high-resolution mesoscale models to simulate precipitation. The precipitation influenced by orography is only well reproduced in the innermost domain, with a horizontal resolution of 5 km. Both distribution and total precipitation amounts are in good accordance with previous studies based on observations, such as AEMET and IPMA (2012), from which the color palette has been reproduced to facilitate the comparison. The results for the other experiments provide very similar geographical distribution but, as previously noted, different precipitation amounts. Higher resolution can improve the results, but the computational cost is very high for long-time simulations used for climate regionalization.

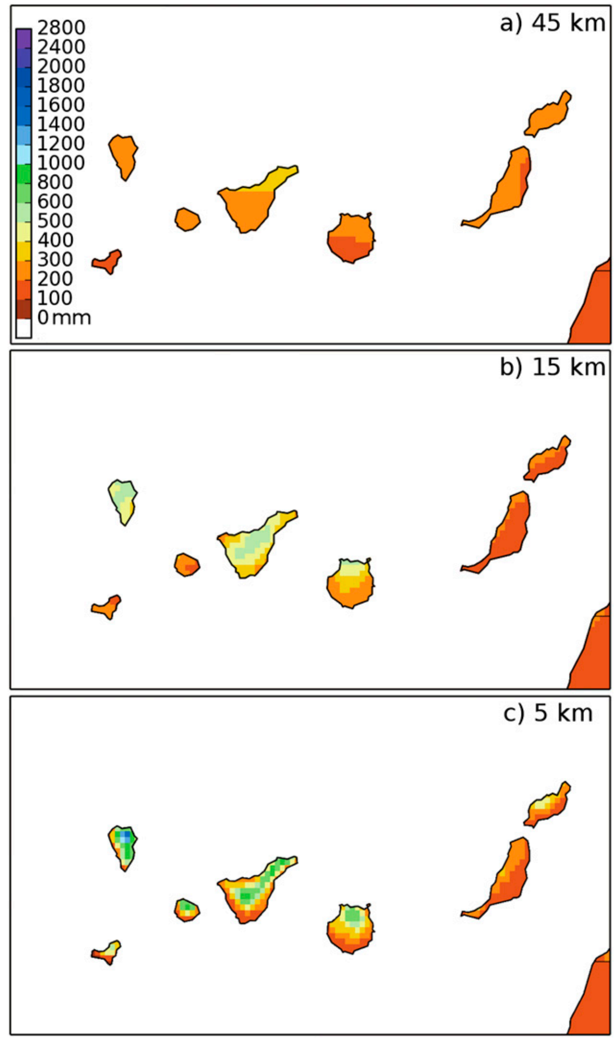


FIG. 7. Mean annual precipitation corresponding to CTRL experiment and computed from the three domain results: (a) D1 with 45-km spatial resolution, (b) D2, and (c) D3. The color palette has been extracted from AEMET and IPMA (2012) to facilitate comparison with their observational studies.

### c. *Daily temperature results*

In this section, the maximum and minimum temperatures obtained through WRF simulations are compared with their respective observational datasets. The selection of maximum and minimum temperatures for the study is because these variables are more relevant than average daily air temperature to environmental processes and climate impacts. The computed maximum and minimum temperatures were carried out thanks to the WRF modification first introduced at the University of Cantabria (Fita et al. 2010), which computes the daily extremes through the values obtained for every simulation time step.

To compare observed and simulated data, both WRF simulated and ERA-Interim temperature data require correction associated with altitude differences between model gridpoint altitudes and the actual locations of the observational stations. This correction was made through a constant lapse rate of $-6.5\ \mathrm{K\,km^{-1}}$, applied to both maximum and minimum temperatures, to minimize the effects of the differences in elevation between the observations and the nearest grid points. This constant lapse rate is a first-order approximation and although far from accurate, because it neglects the local effects on temperature, it was applied to provide a more realistic comparative. It should be noted that altitude corrections were not applied for the precipitation case,

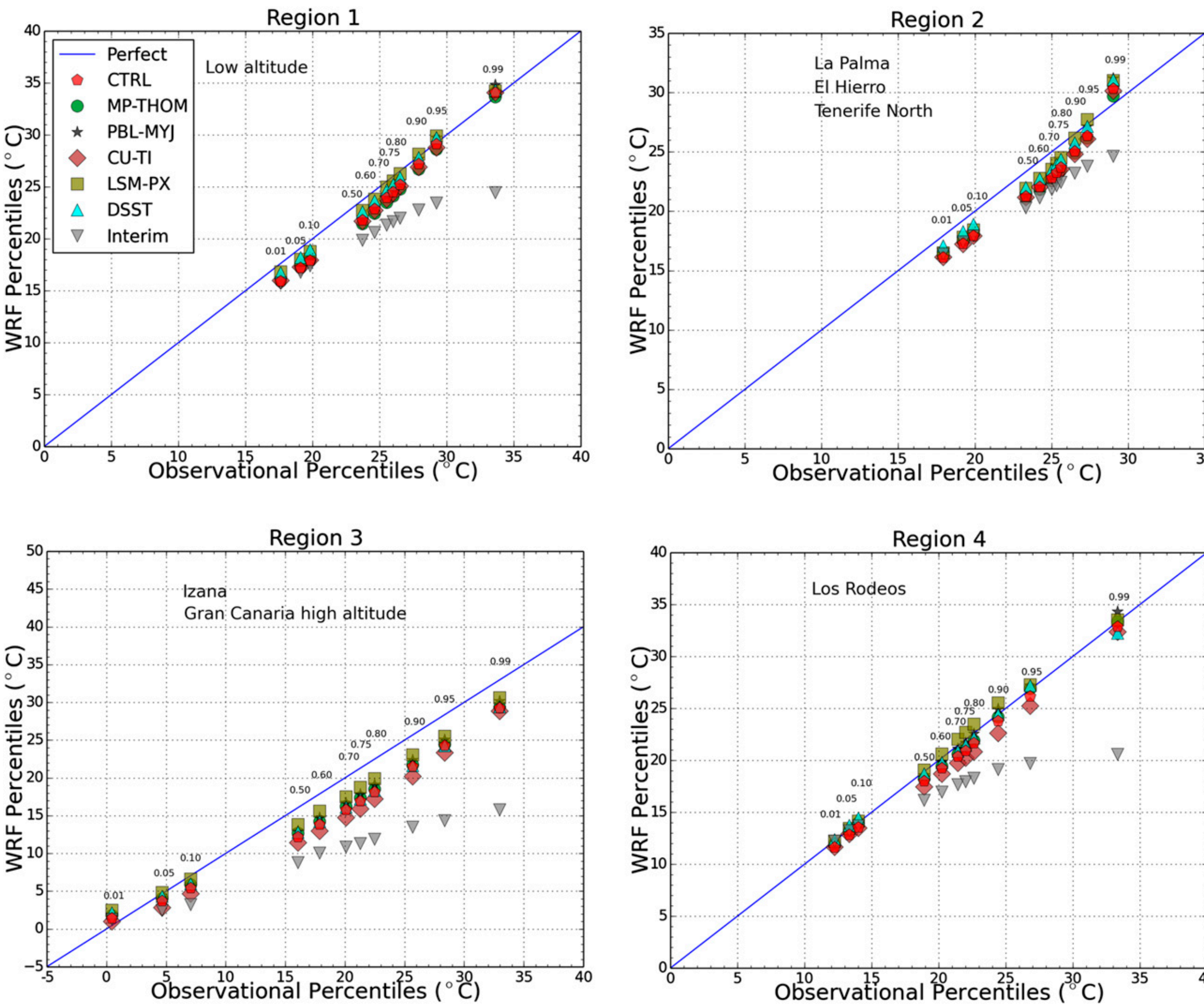


FIG. 8. Percentiles of daily maximum temperature for the five WRF simulations and ERA-Interim vs observational percentiles of each temperature region shown in Fig. 2b. Blue line represents the perfect performance.

because this correction is quite difficult given its dependence on topography, humidity, buoyancy, and other variables (Smith and Barstad 2004).

Maximum and minimum temperature percentiles (the 1st, 5th, 10th, 25th, 75th, 90th, 95th, and 99th) of daily values for the four temperature regions were calculated. The graphical results are shown in Figs. 8 and 9, for maximum and minimum temperatures, respectively, in which percentiles for the WRF simulations versus observational percentiles are presented. As in the case of precipitation, the blue line represents the perfect description, indicating the over- or underestimation of the simulations. Percentiles from ERA-Interim temperatures are also shown. Both maximum and minimum percentiles are accurately captured by WRF, with a clear improvement over ERA-Interim. Notable is the ability of WRF simulations to reproduce the extreme percentiles. The maximum temperature in regions 1 and 2 are very well reproduced by the LSM-PX model, with a slight underestimation for percentiles lower than 75% and an overestimation for higher percentiles. In region 4, LSM-PX overestimates the maximum percentiles, and the other schemes underestimate them, but all follow the observational pattern. The sensitivity of the analyzed results to the SST increment is also remarkable. As expected, temperatures in the near-shore locations are more influenced by these variations than those high-altitude sites, showing increments close to 0.7°C, which corresponds to the mean value added to the ERA-Interim SST in the DSST experiment.

For all simulations, percentiles corresponding to region 3 underestimate temperatures. This behavior could be due to the insufficient temperature correction of $-6.5\,\mathrm{K\,km^{-1}}$. Region 3 corresponds to high

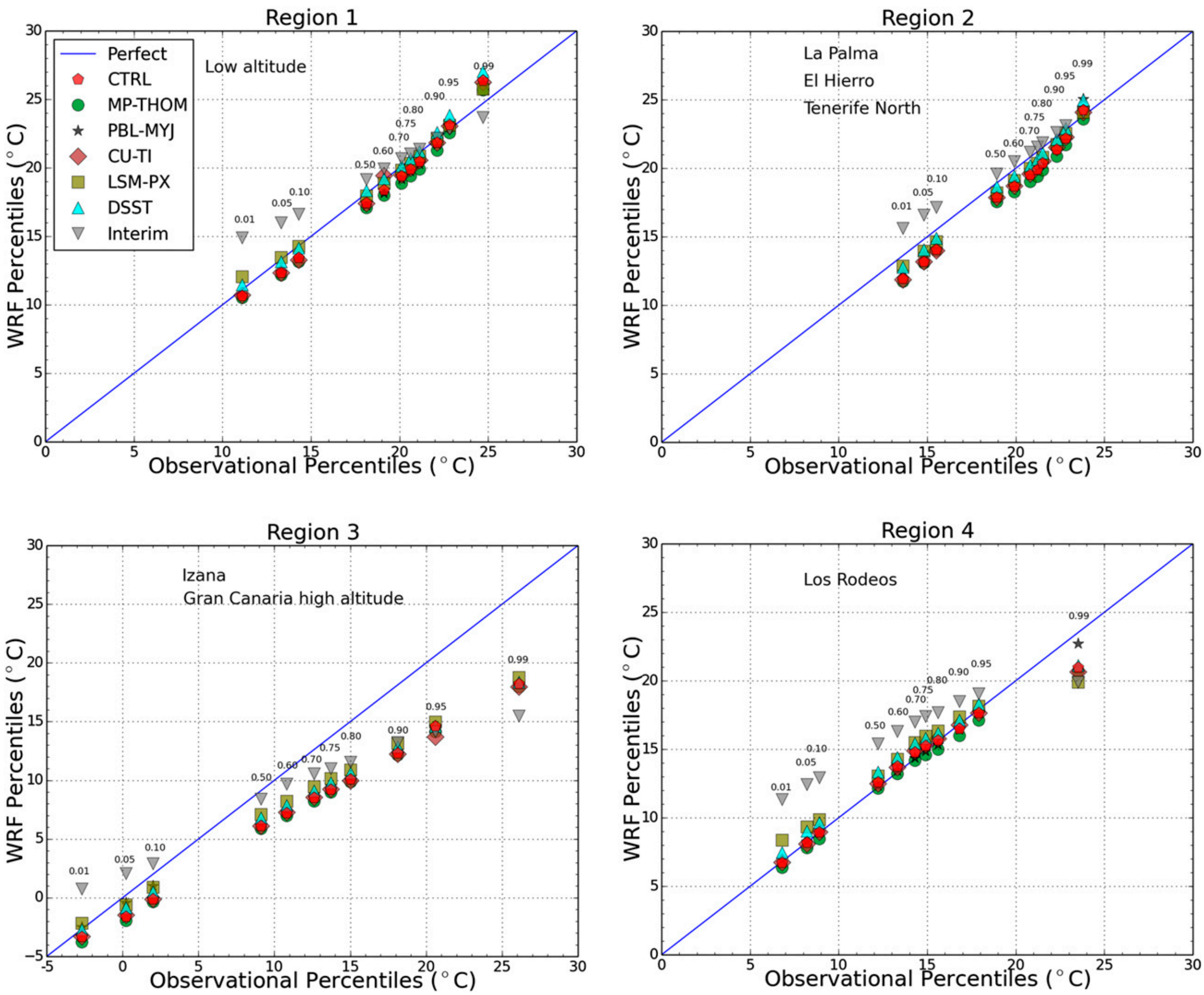


FIG. 9. As in Fig. 8, but for daily minimum temperature.

mountainous areas in Tenerife and Gran Canaria, where a temperature inversion takes place, which corresponds to a positive environmental lapse rate. Minder et al. (2010) found that assumption of a uniform and constant surface lapse rate of $-6.5\,\mathrm{K\,km^{-1}}$ is not a correct representation for mountainous areas, and regional variations in lapse rates and their seasonality should be considered. In the rest of the regions this correction is also important, because the differences in vertical locations between WRF grid points and observational stations are remarkable. The only exception is for Los Rodeos (region 4), where this altitude difference is very small and practically has no effect on the temperature correction.

### *d. Annual cycle for temperature*

The annual cycle for maximum and minimum temperatures is displayed in Fig. 10. These temperatures were computed as the monthly average of daily maximum and minimum temperatures, which were then averaged over the 5-yr period. The observational seasonalities are precisely captured in each region, and the summer peaks are clearly identified. In general, WRF simulations present a slight underestimation, especially in region 3. The only overestimation is observed in region 4, corresponding to LSM-PX. Both overestimation and underestimation in simulated temperature are related to the altitude differences between WRF grid points and observational stations. For the same reason of altitude differences, simulated curves in region 4 are accurately reproduced in WRF experiments, because the altitude difference in this case is on the order of few meters. All the WRF simulations outperform temperature outputs from the ERA-Interim. In general, ERA-Interim annual cycles corresponding to the minimum temperatures are over the observational cycles, whereas the ERA-Interim

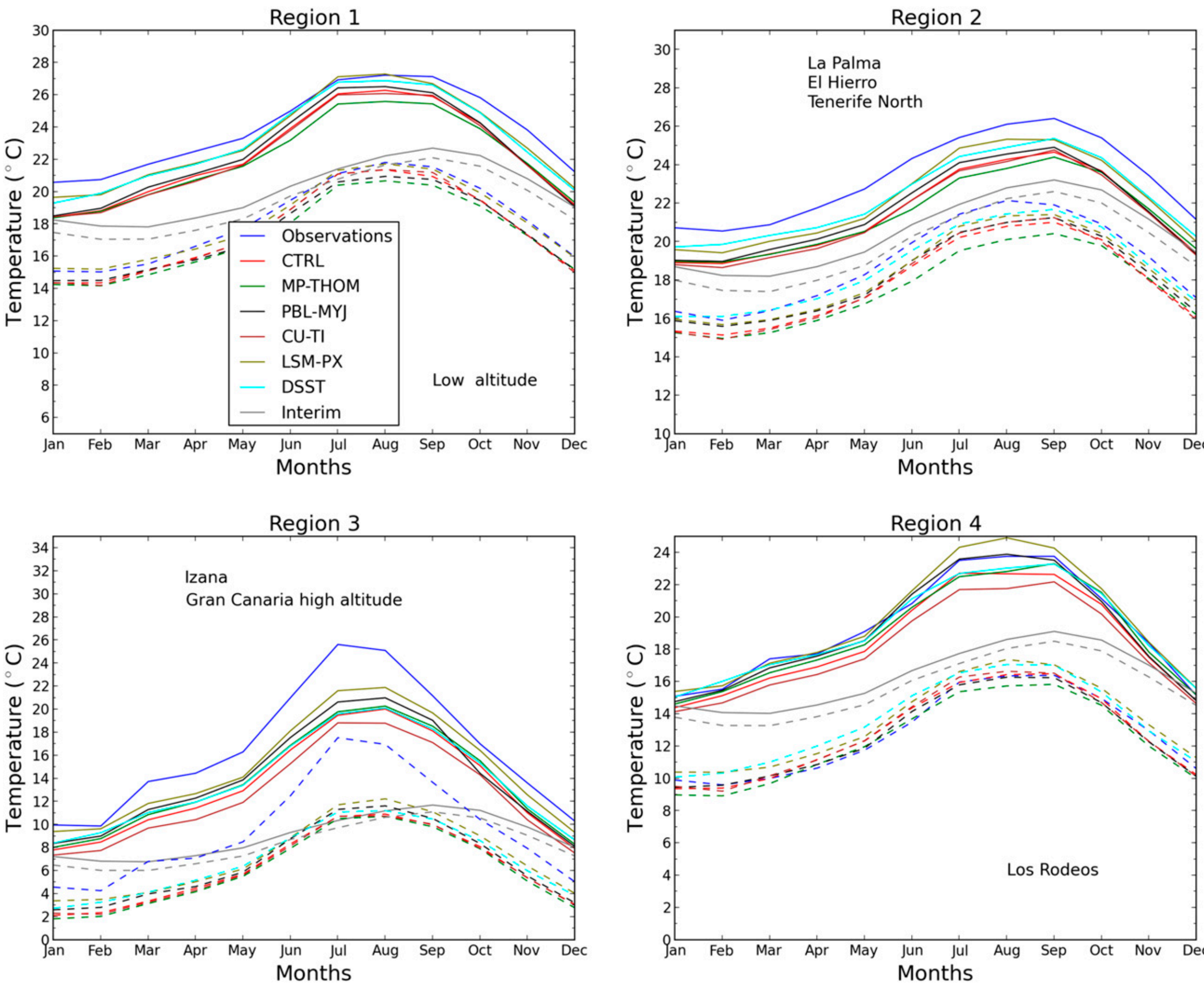


FIG. 10. Annual cycle of monthly maximum (solid line) and minimum (dashed line) temperatures for the different regions shown in Fig. 2b.

annual cycles of the maximum temperatures underestimate if compared with the data provided by observational stations. The best simulation in regions 1, 2, and 3 corresponds to LSM-PX and in region 4 the best results are provided by PBL-MYJ. The temperature increment for the DSST experiment, compared to CTRL simulation, is also observed for those low-altitude regions.

### e. *Statistical study of monthly precipitation and temperature*

Taylor diagrams (Taylor 2001) provide a graphical way to summarize how closely the WRF simulations match the observational data. In this type of polar diagram (see Figs. 11–13) the angular coordinate corresponds to the correlation coefficient between simulated and observed data. The radial coordinate gives information about the standard deviation of the results for each experiment. The black points on the abscissa axis represent the observations. The centered root-mean-square errors (CRMSE) between the experiments and observations are proportional to the distance between this reference and the simulation points. In conclusion, Taylor diagrams are a powerful tool that summarizes three statistics: standard deviation, pattern correlation, and CRMSE, giving a rapid, concise, and easy visual point of view between models and observations. In addition to the before mentioned statistical information, the simulation marks have been colored to represent bias between WRF and the observational series. That simulation closest to the observational mark (largest correlation, smaller CRMSE, and comparable variance) and with white color (low bias) will be the best one. The same statistical procedure was adopted with ERA-Interim in order to evaluate the improvement associated with WRF.

Statistics for the six experiments, together with the ERA-Interim data, were computed for each region and

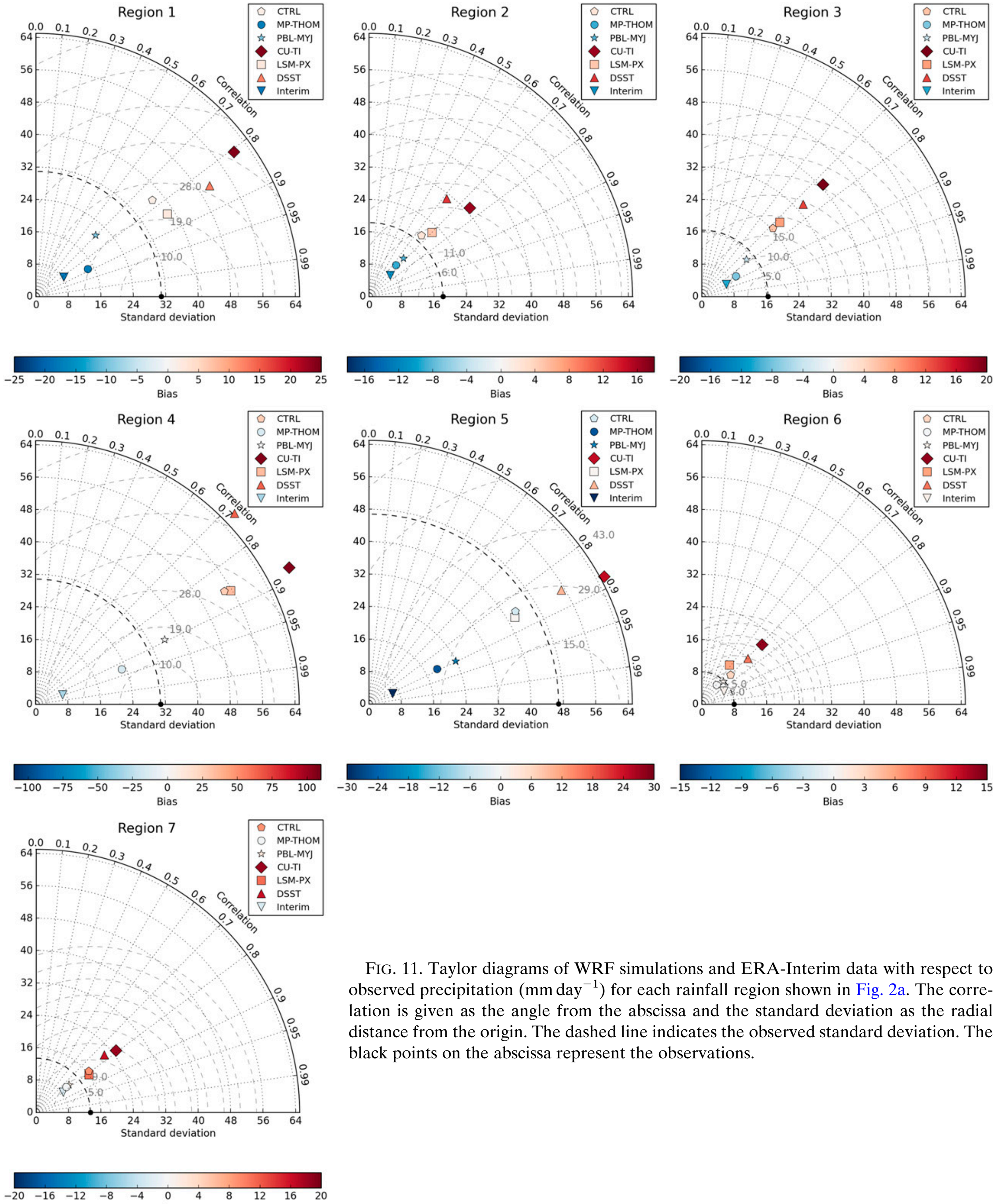


FIG. 11. Taylor diagrams of WRF simulations and ERA-Interim data with respect to observed precipitation (mm day$^{-1}$) for each rainfall region shown in Fig. 2a. The correlation is given as the angle from the abscissa and the standard deviation as the radial distance from the origin. The dashed line indicates the observed standard deviation. The black points on the abscissa represent the observations.

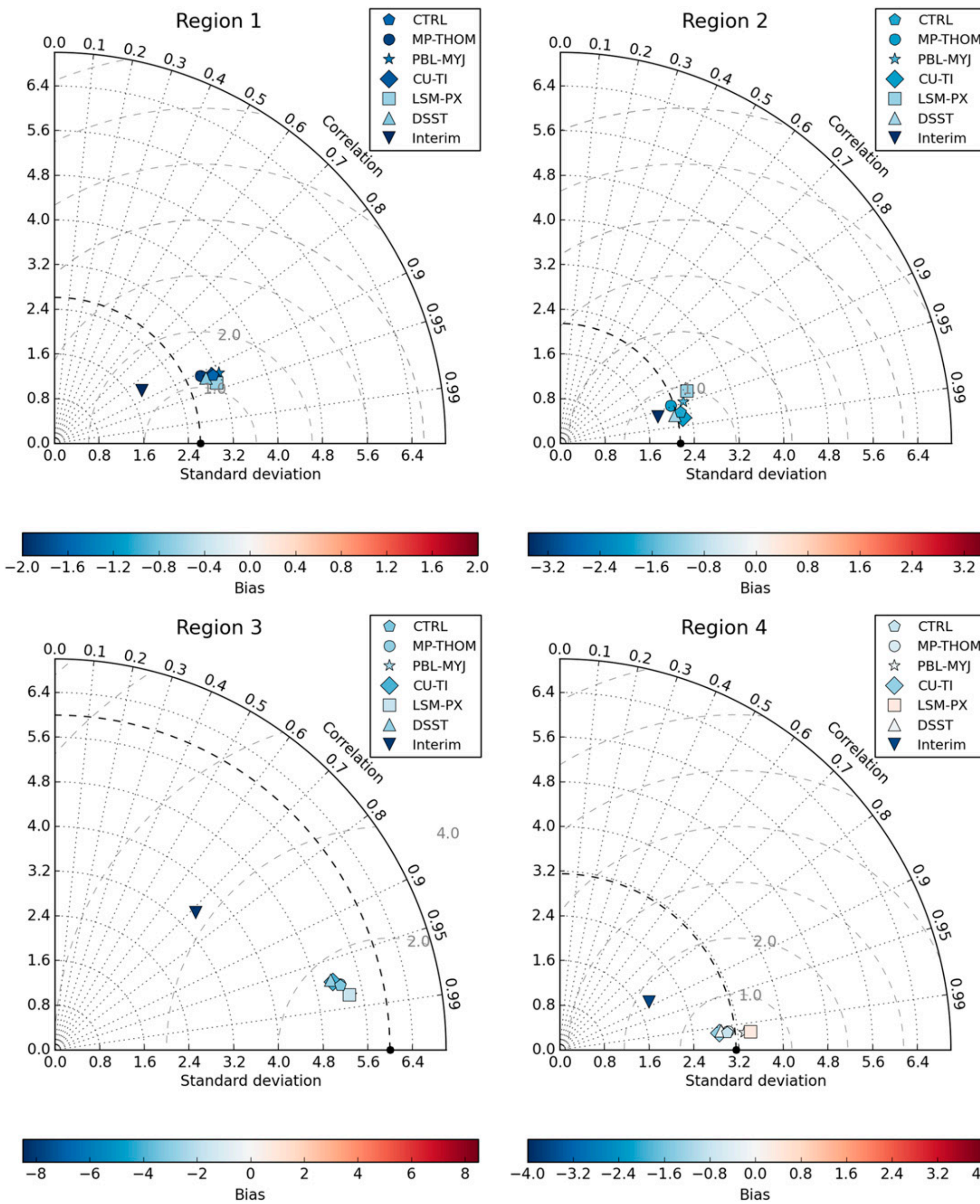


FIG. 12. Taylor diagrams of WRF simulations and ERA-Interim data with respect to observed maximum temperatures for the regions shown in Fig. 2b.

are displayed in Figs. 11–13. Precipitation statistical results (Fig. 11), in some cases, show a smaller standard deviation and RMSE, a slightly better correlation, and lower bias than ERA-Interim. The correlation coefficients vary from 0.55 to 0.95 and CRMSE values range from 3 to 40. CTRL, CU-TI, LSM-PX, and DSST tend to overestimate the precipitation, whereas MP-THOM, PBL-MYJ, and ERA-Interim usually underestimate them. The CU-TI bias overestimations are very high, which was also observed in the annual cycles and in the analysis of hydrometeors mixing ratios. Among all the schemes, the CTRL and PBL-MYJ simulations present the lowest deviations in this sense. It is worth noting that the Taylor diagram presented can be negatively affected by outliers typical of the precipitation field, such as strong rainfall events.

The correlation, CRMSE, standard deviation, and bias are summarized in Figs. 12 and 13 for maximum and minimum temperatures, respectively. These figures represent a comparative study between WRF and

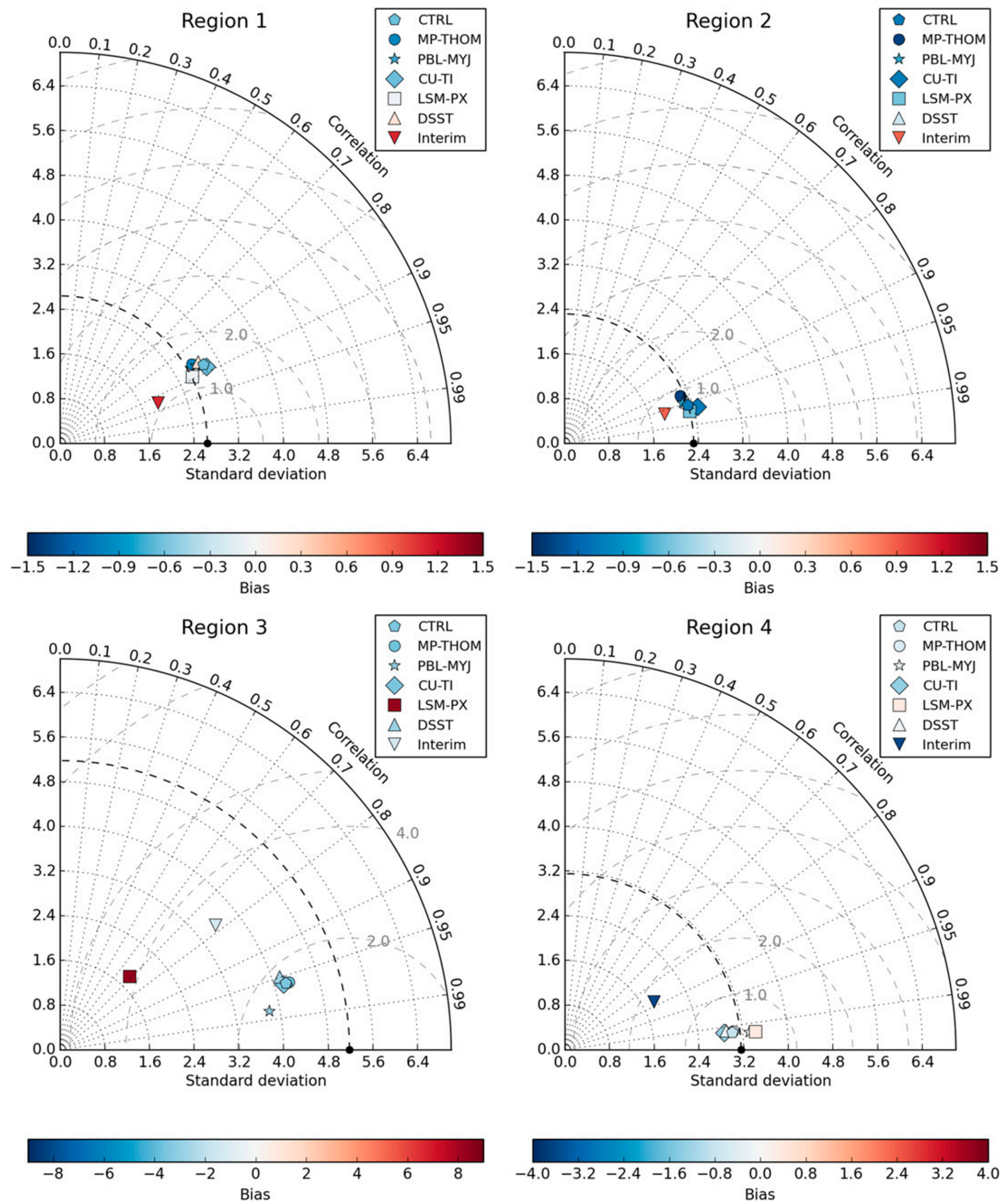


FIG. 13. As in Fig. 13, but for observed minimum temperatures.

observational monthly means, together with ERA-Interim data. In the case of maximum temperatures, the correlation coefficients are over 90%, outperforming ERA-Interim values in regions 1, 3, and 4. In this case, WRF clearly improves the temporal correlation, contrary to the behavior of simulated precipitation, where the correlation to observations is similar for the ERA-Interim and WRF results, suggesting that the timing of precipitation is strongly controlled by the forcing fields. For the minimum temperature, the correlations are above 80%, but without remarkable improvement with respect to ERA-Interim. In all situations, the standard deviation is very close to observational data, and much better than ERA-Interim. Although it is difficult to choose one scheme as the best one for reproducing monthly-mean maximum and minimum temperatures, the LSM-PX simulation could be a good configuration, attending to the bias (except in region 3 for the minimum temperature), although the rest of the experiments present similar results.

## 5. Conclusions

In this work, six different WRF configurations were used to perform dynamical downscaling in order to study temperature and rainfall variables over the complex region of the Canary Islands, using 5-yr continuous runs. The validation of simulations was carried out comparing the simulated results with the observational data provided by meteorological stations and with ERA-Interim data employed as initial and boundary conditions. To facilitate comparison with observations from meteorological stations, a geographical regionalization method has been proposed. It is based on principal component analysis followed by a nonparametric clustering technique, which is able to estimate the number of clusters and to separate them independently on their shape. The simulations demonstrate an improvement in temperature and precipitation fields with respect to ERA-Interim data. In general, physics parameterizations have less effect on temperature than on precipitation, and major discrepancies of WRF estimations, after comparison with station data, were found with respect to rainfall. A detailed study was performed to analyze the differences in the simulated precipitation between the evaluated schemes. Focused on the island of Tenerife, the vertical distribution of the different hydrometeors was studied, observing large discrepancies in the water vapor amount available in the finer domain when different cumulus parameterizations schemes are used in the outermost domain, or when the SST increases. Furthermore, it is also remarkable the differences between the microphysics schemes in the efficiencies of producing precipitation from the water species considered in the scheme. From the set of simulations carried out in this work, the best configuration for precipitation simulation is CTRL, which corresponds to the combination of parameterizations including WDM6, YSU, Noah, and KF. For temperature, the best physical configuration could be with WDM6, YSU, PX, and KF, denoted LSM-PX. For future climate simulations, the LSM-PX and CTRL schemes are recommended because these parameterizations represent correctly temperature and precipitation in the Canary Islands. Moreover, given the small differences of LSM-PX with respect to the other experiments in temperature simulations, and taking into account the good results of CTRL in precipitation, this last could be a good choice for future simulations if the Noah LSM scheme is desired given its flexibility to change land cover properties. Furthermore, the sensitivity of these simulated variables to uncertainties in the prescribed SST was also analyzed, showing that in this kind of region, where the ocean occupies a large portion of the domain, the accuracy of simulated precipitation and temperature depends on the quality of the input data, especially in the near-shore areas for temperature. The variations in simulated precipitation and temperature due to the SST uncertainties used in this work, with an average increment of 0.7°C, are of the same order of those obtained when some parameterizations are changed. However, only five experiments have been performed, choosing those parameterizations that showed better performance in previous studies for the Canary Islands region, and in each of these simulations only one scheme, with respect to the control experiment, was changed at a time. Therefore the feedbacks between the different physical parameterizations, which are also significant, have not been addressed in this study.

*Acknowledgments.* The authors thank the CLIMATIQUE Project, Observatorio Cambio Climático Canarias-Souss Massa Drâa, co-financed by the Programa de Cooperación Transfronteriza España-Fronteras Exteriores 2008-2013 (POCTEFEX) and the European Union funds under Program FEDER, for the economic support. The authors also acknowledge the MEC (Ministry of Education and Science, Spain) for support for projects CGL2010-21366-C04-01 and CGL2010-22158-C02-01. The weather station's data were obtained from the Meteorological State Agency of Spain (AEMET) and the ERA-Interim data were provided by the European Centre for Medium-Range Weather Forecasts (ECMWF). We also acknowledge the World Climate Research Programme's Working Group on Coupled Modelling, which is responsible for CMIP, and we thank the climate modeling groups for producing and making available their model output. For CMIP the U.S. Department of Energy's Program for Climate Model Diagnosis and Intercomparison provides coordinating support and led development of software infrastructure in partnership with the Global Organization for Earth System Science Portals. Detailed comments from the anonymous reviewers are deeply appreciated.

REFERENCES

AEMET and IPMA, 2012: Climate atlas of the archipelagos of the Canary Islands, Madeira and the Azores. State Meteorological Agency of Spain and Institute of Meteorology of Portugal, 80 pp. [Available online at http://www.aemet.es/documentos/es/conocermas/publicaciones/2Atlas_climatologico/Atlas_Clima_Macaronesia___Baja.pdf.]

Argüeso, D., J. M. Hidalgo-Muñoz, S. R. Gámiz-Fortis, M. J. Esteban-Parra, J. Dudhia, and Y. Castro-Díez, 2011: Evaluation of WRF parameterizations for climate studies over southern Spain using a multistep regionalization. *J. Climate,* **24,** 5633–5651, doi:10.1175/JCLI-D-11-00073.1.

Chang, H.-I., A. Kumar, D. Niyogi, U. C. Mohanty, F. Chen, and J. Dudhia, 2009: The role of land surface processes on the mesoscale simulation of the July 26, 2005, heavy rain event over Mumbai, India. *Global Planet. Change,* **67,** 87–103, doi:10.1016/j.gloplacha.2008.12.005.

Chen, F., and J. Dudhia, 2001: Coupling an advanced land surface–hydrology model with the Penn State–NCAR MM5 modeling system. Part I: Model description and implementation. *Mon. Wea. Rev.,* **129,** 569–585, doi:10.1175/1520-0493(2001)129<0569:CAALSH>2.0.CO;2.

Collins, W. D., and Coauthors, 2004: Description of the NCAR Community Atmosphere Model (CAM3.0). NCAR Tech. Note NCAR/TN-464+STR, 226 pp.

Crétat, J., B. Pohl, Y. Richard, and P. Drobinski, 2012: Uncertainties in simulating regional climate of southern Africa: Sensitivity to physical parameterizations using WRF. *Climate Dyn.,* **38,** 613–634, doi:10.1007/s00382-011-1055-8.

Daszykowski, M., B. Walczak, and D. L. Massart, 2001: Looking for natural patterns in data: Part 1. Density-based approach. *Chemometr. Intell. Lab. Syst.,* **56,** 83–92, doi:10.1016/S0169-7439(01)00111-3.

Dee, D. P., and Coauthors, 2011: The ERA-Interim reanalysis: Configuration and performance of the data assimilation system. *Quart. J. Roy. Meteor. Soc.,* **137,** 553–597, doi:10.1002/qj.828.

Díez, E., C. Primo, J. A. García-Moya, J. M. Gutiérrez, and B. Orfila, 2005: Statistical and dynamical downscaling of precipitation over Spain from DEMETER seasonal forecasts. *Tellus,* **57A,** 409–423, doi:10.1111/j.1600-0870.2005.00130.x.

Dulière, V., Y. Zhang, and E. P. Salathé, 2011: Extreme precipitation and temperature over the U.S. Pacific Northwest: A comparison between observations, reanalysis data, and regional models. *J. Climate,* **24,** 1950–1964, doi:10.1175/2010JCLI3224.1.

Ester, M., H.-P. Kriegel, J. Sander, and X. Xu, 1996: A density-based algorithm for discovering clusters in large spatial databases with noise. *Proc. Second Int. Conf. on Knowledge Discovery and Data Mining,* Portland, OR, AAAI, 226–231.

Evans, J. P., and M. F. McCabe, 2010: Regional climate simulation over Australia's Murray-Darling basin: A multitemporal assessment. *J. Geophys. Res.,* **115,** D14114, doi:10.1029/2010JD013816.

——, M. Ekström, and F. Ji, 2012: Evaluating the performance of a WRF physics ensemble over South-East Australia. *Climate Dyn.,* **39,** 1241–1258, doi:10.1007/s00382-011-1244-5.

Fita, L., J. Fernández, and M. García-Díez, 2010: CLWRF: WRF modifications for regional climate simulation under future scenarios. Preprints, *11th WRF Users' Event,* Boulder, CO, NCAR, P-26. [Available online at http://www.meteo.unican.es/en/node/72915.]

Flaounas, E., S. Bastin, and S. Janicot, 2011: Regional climate modelling of the 2006 West African monsoon: Sensitivity to convection and planetary boundary layer parameterisation using WRF. *Climate Dyn.,* **36,** 1083–1105, doi:10.1007/s00382-010-0785-3.

Font-Tullot, I., 1956: *El tiempo atmosférico en las Islas Canarias*. Servicio Meteorológico National Publicaciones, Serie A (Memorias), Vol. 26, 88 pp.

Fowler, H. J., S. Blenkinsop, and C. Tebaldi, 2007: Linking climate change modelling to impacts studies: Recent advances in downscaling techniques for hydrological modelling. *Int. J. Climatol.,* **27,** 1547–1578, doi:10.1002/joc.1556.

García-Herrera, R., D. Gallego, E. Hernández, L. Gimeno, and P. Ribera, 2001: Influence of the North Atlantic Oscillation on the Canary Islands precipitation. *J. Climate,* **14,** 3889–3903, doi:10.1175/1520-0442(2001)014<3889:IOTNAO>2.0.CO;2.

Giorgi, F., and Coauthors, 2001: Regional climate information—Evaluation and projections. *Climate Change 2001: The Scientific Basis,* J. T. Houghton et al., Eds., Cambridge University Press, 583–638.

González, A., F. C. Expósito, J. Pérez, J. P. Díaz, and D. Taima, 2013: Verification of precipitable water vapour in high-resolution WRF simulations over a mountainous archipelago. *Quart. J. Roy. Meteor. Soc.,* **139,** 2119–2133, doi:10.1002/qj.2092.

Grell, G. A., J. Dudhia, and D. R. Stauffer, 1995: A description of the fifth-generation Penn State/NCAR Mesoscale Model (MM5). NCAR Tech. Note NCAR/TN-398+STR, 122 pp.

Hamdi, R., H. Van de Vyver, R. De Troch, and P. Termonia, 2014: Assessment of three dynamical urban climate downscaling methods: Brussels's future urban heat island under an A1B emission scenario. *Int. J. Climatol.,* **34,** 978–999, doi:10.1002/joc.3734.

Hong, S.-Y., and J.-O. J. Lim, 2006: The WRF single-moment 6-class microphysics scheme (WSM6). *J. Korean Meteor. Soc,* **42** (2), 129–151.

——, Y. Noh, and J. Dudhia, 2006: A new vertical diffusion package with an explicit treatment of entrainment processes. *Mon. Wea. Rev.,* **134,** 2318–2341, doi:10.1175/MWR3199.1.

Janjić, Z. I., 2002: Nonsingular implementation of the Mellor-Yamada level 2.5 scheme in the NCEP-Meso model. NCEP Office Note 437, 61 pp.

Jiménez, P., E. García-Bustamante, J. F. González-Rouco, F. Valero, J. Montávez, and J. Navarro, 2008: Surface wind regionalization in complex terrain. *J. Appl. Meteor. Climatol.,* **47,** 308–325, doi:10.1175/2007JAMC1483.1.

Kain, J. S., and J. M. Fritsch, 1990: A one-dimensional entraining/detraining plume model and its application in convective parameterization. *J. Atmos. Sci.,* **47,** 2784–2802, doi:10.1175/1520-0469(1990)047<2784:AODEPM>2.0.CO;2.

Kaufman, L., and P. J. Rousseeuw, 1990: *Finding Groups in Data: An Introduction to Cluster Analysis*. Wiley, 342 pp.

Köppen, W., 1936: Das geographische System der Klimate. *Handbuch der Klimatologie,* Vol. 1, Part C, C. Köppen and R. Geiger, Eds., Gebrüder Bornträger, 1–44.

Leung, L. R., L. O. Mearns, F. Giorgi, and R. L. Wilby, 2003: Regional climate research: Needs and opportunities. *Bull. Amer. Meteor. Soc.,* **84,** 89–95, doi:10.1175/BAMS-84-1-89.

Lim, K.-S. S., and S.-Y. Hong, 2010: Development of an effective double-moment cloud microphysics scheme with prognostic cloud condensation nuclei (CCN) for weather and climate models. *Mon. Wea. Rev.,* **138,** 1587–1612, doi:10.1175/2009MWR2968.1.

Lo, J. C.-F., Z.-L. Yang, and R. A. Pielke, 2008: Assessment of three dynamical climate downscaling methods using the Weather Research and Forecasting (WRF) model. *J. Geophys. Res.,* **113,** D09112, doi:10.1029/2007JD009216.

Martín, J. L., J. Bethencourt, and E. Cuevas-Agulló, 2012: Assessment of global warming on the island of Tenerife, Canary Islands (Spain). Trends in minimum, maximum and mean temperatures since 1944. *Climatic Change,* **114,** 343–355, doi:10.1007/s10584-012-0407-7.

Miguez-Macho, G., G. L. Stenchikov, and A. Robock, 2004: Spectral nudging to eliminate the effects of domain position and geometry in regional climate model simulations. *J. Geophys. Res.,* **109,** D13104, doi:10.1029/2003JD004495.

Minder, J. R., P. W. Mote, and J. D. Lundquist, 2010: Surface temperature lapse rates over complex terrain: Lessons from the Cascade Mountains. *J. Geophys. Res.,* **115,** D14122, doi:10.1029/2009JD013493.

Mooney, P. A., F. J. Mulligan, and R. Fealy, 2011: Comparison of ERA-40, ERA-Interim and NCEP/NCAR reanalysis data with observed surface air temperatures over Ireland. *Int. J. Climatol.,* **31,** 545–557, doi:10.1002/joc.2098.

Nikulin, G., and Coauthors, 2012: Precipitation climatology in an ensemble of CORDEX-Africa regional climate simulations. *J. Climate,* **25,** 6057–6078, doi:10.1175/JCLI-D-11-00375.1.

Pohl, B., J. Crétat, and P. Camberlin, 2011: Testing WRF capability in simulating the atmospheric water cycle over equatorial East Africa. *Climate Dyn.,* **37,** 1357–1379, doi:10.1007/s00382-011-1024-2.

Radu, R., M. Déqué, and S. Somot, 2008: Spectral nudging in a spectral regional climate model. *Tellus,* **60A,** 898–910, doi:10.1111/j.1600-0870.2008.00341.x.

Simmons, A., S. Uppala, D. Dee, and S. Kobayashi, 2006: ERA-Interim: New ECMWF reanalysis products from 1989 onwards. *ECMWF Newsletter,* No. 110, ECMWF, Reading, United Kingdom, 26–35.

Skamarock, W. C., and Coauthors, 2008: A description of the Advanced Research WRF version 3. NCAR Tech. Note NCAR/TN-475+STR, 125 pp.

Smith, R. B., and I. Barstad, 2004: A linear theory of orographic precipitation. *J. Atmos. Sci.,* **61,** 1377–1391, doi:10.1175/1520-0469(2004)061<1377:ALTOOP>2.0.CO;2.

Soriano, C., O. Jorba, and J. M. Baldasano, 2002: One-way nesting versus two-way nesting: Does it really make a difference? *Air Pollution Modelling and Its Application XV,* C. Borrego and G. Schayes, Eds., Kluwer Academic, 177–185.

Stauffer, D. R., and N. L. Seaman, 1990: Use of four-dimensional data assimilation in a limited-area forecast model. Part I: Experiments with synoptic-scale data. *Mon. Wea. Rev.,* **118,** 1250–1277, doi:10.1175/1520-0493(1990)118<1250:UOFDDA>2.0.CO;2.

Suklitsch, M., A. Gobiet, H. Truhetz, N. K. Awan, H. Göttel, and D. Jacob, 2011: Error characteristics of high-resolution regional climate models over the Alpine area. *Climate Dyn.,* **37,** 377–390, doi:10.1007/s00382-010-0848-5.

Taylor, K. E., 2001: Summarizing multiple aspects of model performance in a single diagram. *J. Geophys. Res.,* **106,** 7183–7192, doi:10.1029/2000JD900719.

Thompson, G., P. R. Field, R. M. Rasmussen, and W. D. Hall, 2008: Explicit forecasts of winter precipitation using an improved bulk microphysics scheme. Part II: Implementation of a new snow parameterization. *Mon. Wea. Rev.,* **136,** 5095–5115, doi:10.1175/2008MWR2387.1.

Thornthwaite, C. W., 1948: An approach toward a rational classification of climate. *Geogr. Rev.,* **38,** 55–94, doi:10.2307/210739.

Wilks, D. S., 2005: *Statistical Methods in the Atmospheric Sciences*. Academic Press, 649 pp.

Xiu, A., and J. E. Pleim, 2001: Development of a land surface model. Part I: Application in a mesoscale meteorological model. *J. Appl. Meteor.,* **40,** 192–209, doi:10.1175/1520-0450(2001)040<0192:DOALSM>2.0.CO;2.

Yuan, X., X.-Z. Liang, and E. F. Wood, 2012: WRF ensemble downscaling seasonal forecasts of China winter precipitation during 1982–2008. *Climate Dyn.,* **39,** 2041–2058, doi:10.1007/s00382-011-1241-8.

Zhang, C., Y. Wang, and K. Hamilton, 2011: Improved representation of boundary layer clouds over the southeast Pacific in WRF-ARW using a modified Tiedtke cumulus parameterization scheme. *Mon. Wea. Rev.,* **139,** 3489–3513, doi:10.1175/MWR-D-10-05091.1.